Bulk Fermi surface mapping with high-energy angle-resolved photoemission

2003 J. Phys.: Condens. Matter 15 6919

(http://iopscience.iop.org/0953-8984/15/41/002)

INSTITUTE OF PHYSICS PUBLISHING JOURNAL OF PHYSICS: CONDENSED MATTER

J. Phys.: Condens. Matter **15** (2003) 6919–6930 PII: S0953-8984(03)64844-7

Bulk Fermi surface mapping with high-energy angle-resolved photoemission

M B Nielsen[1], Z Li[1], S Lizzit[2], A Goldoni[2] and Ph Hofmann[1,3]

[1] Institute for Storage Ring Facilities, University of Aarhus, DK-8000 Aarhus C, Denmark
[2] Sincrotrone Trieste, S S 14 Km 163.5, 34012 Trieste, Italy

E-mail: philip@phys.au.dk

Received 15 June 2003
Published 3 October 2003
Online at stacks.iop.org/JPhysCM/15/6919

Abstract

We have studied the Fermi surface of copper by angle-resolved photoemission for photon energies between 95.37 and 259.6 eV. Fermi surface images were obtained by scanning the polar emission angle as well as the photon energy while monitoring the photoemission intensity at the Fermi level. Such images are distorted because of the non-conservation of the perpendicular k component in photoemission. However, if the scans are performed such that the k steps parallel to the surface are identical for all photon energies, the distortion can be corrected for using appropriate final states, for example free-electron final states. We find reasonable agreement between our results and the well-known Fermi surface of copper.

M This article features online multimedia enhancements

1. Introduction

Many fundamental properties of a metal are determined by the shape of its Fermi surface. The most important experimental technique for determining the Fermi surface is based on the de Haas–van Alphen effect, i.e. on the observation of quantum oscillations in the sample's magnetic susceptibility. This and related effects have been successfully applied to map the Fermi surfaces of many metals. There are, however, some severe restrictions. One is that the observation of the quantum oscillations requires very pure samples, low temperatures and high magnetic fields. Another is that the effect cannot be observed at all for certain types of metals, for example for alloys or for materials which are only metals above a certain (high) temperature. Finally, difficulties can arise in the case of low-dimensional systems, in particular when the Fermi surface lacks closed orbits [1].

[3] http://www.phys.au.dk/~philip

An alternative approach to Fermi surface determination is angle-resolved photoemission spectroscopy (ARPES). This technique is capable of mapping the three-dimensional band structure of a solid and the Fermi surface can be viewed as a by-product of a complete mapping experiment. Indeed, ARPES can also provide a direct image of the Fermi surface when the photoemission intensity in a narrow energy window around the Fermi level is displayed as a function of emission angle or photon energy [2–5]. In the rest of this paper we refer to this image as the 'Fermi contour'. This idea has been successfully applied to many systems. However, it has been found that the simple identification of intensity maxima with Fermi surface positions can lead to systematic qualitative and quantitative errors, in particular for narrow-band systems, and several strategies have been developed in order to cure this problem [6–8].

The Fermi surface determination by ARPES appears to work especially well for quasi two-dimensional systems like electronic surface states [9], or layered compounds with little dispersion of the electronic states perpendicular to the layers [2, 4, 6]. This is mainly due to the fact that the perpendicular component of k, $k_\perp$, is not a good quantum number for a semi-infinite crystal and it is not conserved as the photoelectron crosses the surface barrier. Therefore it is not trivial to infer the desired $k_\perp$ inside the crystal from the measured $k_\perp$ outside. This problem is well known from three-dimensional band structure mapping experiments with ARPES [10]. However, $k_\perp$ inside the crystal can be recovered by using an appropriate model for the final states. In practice, free-electron final states are frequently assumed, despite the fact that they may not be appropriate for the low-lying final states. A more sophisticated approach is to use final state bands which have been determined by calculations or experimentally by very low-energy electron diffraction (VLEED) [11]. A different, but related, difficulty arises from the fact that states with a dispersion in the direction perpendicular to the surface give rise to much broader peaks in ARPES than states for which such a dispersion is absent [12]. This complicates the task of precise crossing point determination.

Nevertheless, three-dimensional Fermi surfaces have also been mapped successfully with ARPES. The most thoroughly studied case is that of copper where an analysis of the data in terms of free-electron final states generally has lead to a reasonable agreement with calculated Fermi surfaces [3, 6, 13–16] and where a direct comparison of the experimental data to more sophisticated calculations within the one-step model of photoemission has even yielded good quantitative agreement [17]. A complication in most of these experiments is that the data have been taken by scanning the electron emission angles at a fixed photon energy. With the data taken in this way, the result is not a cut through the Fermi surface in a high-symmetry plane but a spherical cut through the three-dimensional Fermi surface (assuming free-electron final states).

In this paper we study the Fermi surface of copper at higher photon energies than usually employed in ARPES. This strategy could have several advantages. First, by extending the measurements to high energies one can substantially increase the total accessible range of $k_\perp$. With high-energy electrons one does not have to go to grazing emission angles in order to measure a high value of $k_\parallel$ and the refraction effect which occurs upon crossing the surface barrier is far less important because the relative difference of the kinetic energies inside and outside the solid is small. In addition to this, the longer electron mean free path at high energies could increase the bulk sensitivity of the experiment (although this has recently been called into question [18]). Finally, employing free-electron final states should be more justified at high energies than at low energies, facilitating the analysis of the data.

On the other hand, there are several possible problems when using high energies. The cross section for photoemission from the valence band decreases with photon energy. Furthermore, the angular resolution of the electron analyser has to be much higher than at low photon energies in order to maintain a certain $k_\parallel$ resolution. The consequence is a relatively low

count rate from the valence band. These problems are more of a technical nature and can be overcome by modern bright synchrotron radiation sources. More fundamental difficulties arise from the fact that phonon scattering causes the direct transition photoemission peaks to disappear at high energies (or high temperatures) and may have a substantial influence on the photoemission lineshape at intermediate temperatures where the peaks have not yet disappeared [19]. However, it should be possible to avoid this by cooling the sample to low temperatures (relative to the Debye temperature).

In our experiment we have used an approach for scanning the photon energy and electron emission angle which differs from most previous Fermi surface determinations by ARPES. We have kept the azimuthal emission angle of the sample fixed and scanned the photon energy and the polar emission angle only. The sample was set into a high-symmetry azimuth and for every photon energy a polar angle scan was performed. The angular steps were calculated such that the same set of $k_\parallel$ values was probed for all photon energies. This procedure results in a Fermi contour which is still distorted, i.e. which consists of a set of intensity at exact $k_\parallel$ and irregular $k_\perp$ values, but at least lies in one high-symmetry plane of the sample. A similar approach was used to map the three-dimensional Fermi surface of Cu and 1 T-$TiTe_2$ by Rotenberg *et al* [15] and Rossnagel *et al* [20], respectively. In fact, in the work of Rotenberg *et al* the photoemission intensity at the Fermi level was measured over an extensive set of energies and angles such that it could be subsequently interpolated in the desired fraction of k space.

2. Experiment

The experiment was performed at the SuperESCA beamline of the synchrotron radiation light source ELETTRA in Trieste. The geometry of the experimental station is such that there is an angle of 40° between the incoming light and the electron energy analyser. For details see [21, 22]. The polished Cu(111) crystal, mounted on a motorized, computer-controlled manipulator with 5 degrees of freedom, was cleaned by cycles of Ar^+ sputtering and annealing until no surface contamination could be found by x-ray photoelectron spectroscopy and a sharp low-energy electron diffraction (LEED) pattern was observed. The sample azimuth was aligned by LEED such that a change of the polar angle corresponded to changing $k_\parallel$ in a $\langle 112 \rangle$ direction. The directions of the polar angle movement are defined such that a negative $k_\parallel$ corresponds to turning the crystal normal towards the synchrotron radiation beam. An fcc(111) surface gives rise to a hexagonal LEED pattern with an intensity distribution which is only three-fold. The absolute orientation of the sample can therefore be determined by a qualitative comparison of the observed LEED $I(V)$ curves to calculations [23]. All photoemission data were taken at room temperature. Normal emission was determined by measuring the dispersion of the well-known Shockley-type surface state at the centre of the surface Brillouin zone. The highest binding energy of this state was determined to be around 300 meV, a value slightly lower than that found in the literature [24]. This difference is probably caused by a slight tilt in the sample orientation which could not be corrected. From the known surface state dispersion this tilt angle can be estimated to be 1.2°.

3. Results and discussion

Figure 1 shows the result of an angular scan at a photon energy of $h\nu = 105.14$ eV. The range of $k_\parallel$ relative to the surface Brillouin zone is marked as a red line in the inset of the figure. The parabolic dispersion of the surface state around normal emission (at $\bar{\Gamma}_1$, $k_\parallel = 0$) can easily be identified. The same state is also seen around the $\bar{\Gamma}_2$ point in the neighbouring surface Brillouin zone. Here it appears broader and does not extend to such high binding energies.

This is due to a slight misalignment of the sample azimuth, consistent with the fact that the state appears to be broader in energy because we did not cut the paraboloid through the centre. This misalignment is of the order of 2°. Apart from the surface states there are several broader and yet unidentified bulk features visible.

The angular resolution of the electron analyser is not known but we can use the surface state lineshape in order to estimate it. It is well known that a finite angular resolution leads to a $k_\parallel$ integration which can severely distort the lineshape of a surface state peak and for a simple system like this one, the expected lineshape can be calculated [12]. It has been shown previously that a comparison of measured and calculated lineshapes can give an estimate of the angular resolution [25] and an application of the same formalism to data such as in figure 1 yields a value of 0.4° for the present system. Indeed, a visual inspection of the data in figure 1 already suggests that the angular resolution must be high because the surface state parabola is clearly visible and appears undistorted despite the high kinetic energy. We can conclude that, in the energy range we explore in this paper, a $k_\parallel$ integration due to poor angular resolution will only be of minor significance.

From 66 scans as shown in figure 1, taken for photon energies between 95.37 and 259.6 eV we can construct figure 2, the photoemission intensity integrated in an energy window of 150 meV width around the Fermi level. The steps in photon energy have been chosen such that they correspond to constant steps in $|k|$ for free electrons. In the raw results of this integration (not shown), all structure in the high-energy part is invisible because the photoemission intensity is much higher at low energies. In addition to this, discontinuities in the intensity are visible which correspond to the interruptions of the experiment during injections of electrons into the storage ring. Such discontinuities could not be avoided entirely despite of the fact that the data have been normalized by the photoemission current of the last mirror in the beamline. Figure 2 shows the normalized version of the data. To obtain this, the discontinuities were first removed manually. Then the average intensity for every row of the picture, i.e. for every photon energy, was determined. These average intensities have been fitted by a smooth function and every row has been divided by the value of this function.

The segments of Fermi contour caused by the surface states are easily identifiable as vertical lines in figure 2, centred around the surface state positions at $\bar{\Gamma}_1$ ($k_\parallel = 0$ Å^{-1}) and $\bar{\Gamma}_2$ ($k_\parallel = -2.84$ Å^{-1}), consistent with the definition of a genuine surface state which has no dispersion with $k_\perp$. The intensity of the surface state and its Fermi level crossings is resonantly enhanced in the vicinity of the bulk Fermi surface 'necks', a fact which is well know and related to the remaining periodicity of the surface state wavefunctions perpendicular to the surface [18, 26].

Emission from bulk states gives rise to several structures in figure 2 which clearly show dispersion with $k_\perp$. At lower photon energies, some of these structures are rather well-defined in k but they become blurred for the higher energies. This can be explained by the increasing importance of indirect transitions in the photoemission process as the sample temperature or the photon energy is increased. In the most simple picture, these indirect transitions decrease the photoemission intensity of the direct transitions while increasing the incoherent background in the photoemission spectra [27]. A more detailed analysis, however, reveals that most of the electrons which have been scattered by one or two phonons still contribute significantly to the direct transition peak and cause an additional broadening at high energies [19].

In figure 3 we compare the measured Fermi contour to the bulk Fermi surface of Cu. The latter has been determined by various techniques giving very similar results [28]. In this work we have used the result from Kamm which was obtained using the magnetoacoustic effect [29]. For our purpose, we could equally well have chosen a Fermi surface as determined by the de Haas–van Alphen effect. For a comparison with our data, we have to determine the

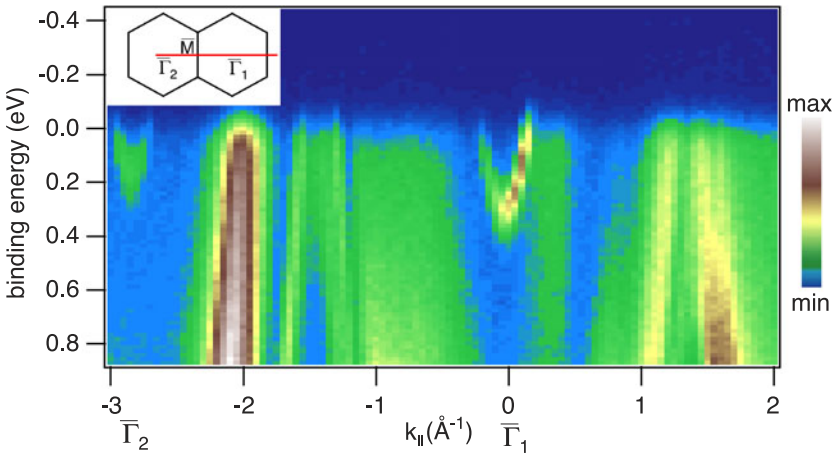

Figure 1. Photoemission intensity as a function of binding energy and $k_{\parallel}$ for a photon energy of $h\nu = 105.14$ eV. The inset shows the surface Brillouin zone with the $k_{\parallel}$ range of the scan indicated as a red line.

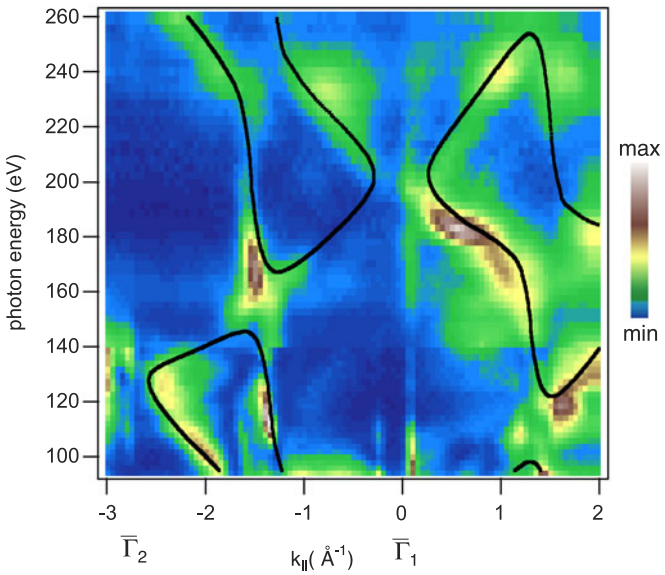

Figure 2. Integrated photoemission intensity at the Fermi level as a function of $k_{\parallel}$ and photon energy. The black curves are the expected bulk Fermi surface crossings, assuming free-electron final states (see text).

absolute value of $k_{\perp}$ for each data point and we do so by using free-electron final states. We have chosen an inner potential of 13.5 eV (including the work function) and an effective mass of one, which is consistent with low-energy photoemission studies from copper [30]. The result is shown in figure 3(a). The agreement between the Fermi contour and the Fermi surface is good for the lower left 'butterfly' but poorer for the upper right 'butterfly'. The overall agreement can be improved somewhat by increasing the inner potential to 19 eV, as shown in figure 3(b) and used throughout the rest of this paper. Nearly the same result can be obtained by choosing an effective mass which is slightly (3%) higher than one while keeping the inner

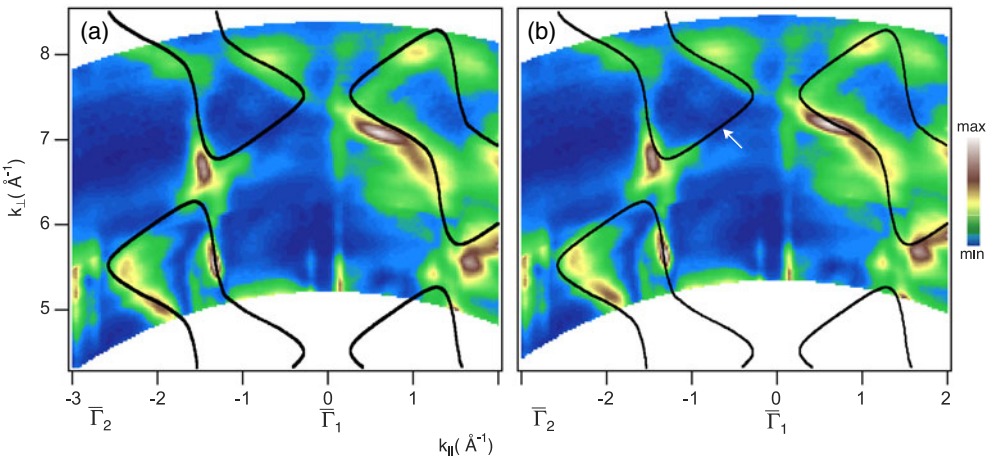

Figure 3. Fermi surface segments of Cu with an interpolation of the data shown in figure 2 using free-electron final states with an inner potential of (a) 13.5 eV and (b) 19 eV. The black curves are the expected bulk Fermi level crossings.

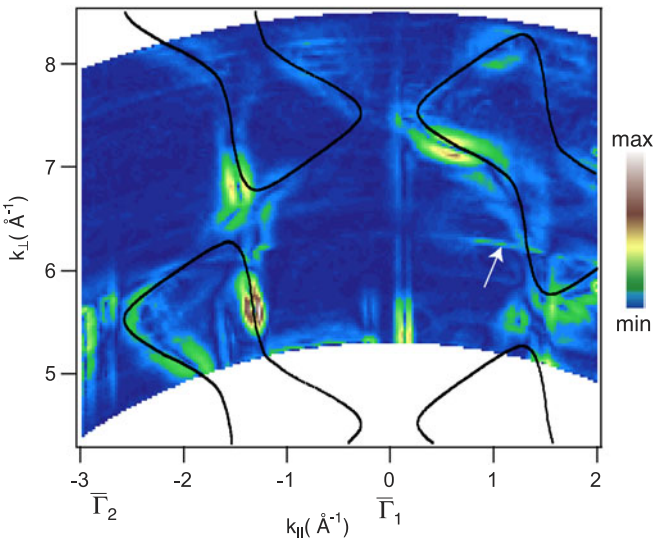

Figure 4. Modulus of the photoemission intensity gradient $|\nabla_k I(k)|$ obtained from the data shown in figure 3(b). The black curves are the expected bulk Fermi surface crossings.

potential at 13.5 eV. In principle one would have to choose an energy-dependent inner potential to account for the energy dependence of the self-energy [31]. Indeed, according to figure 3 different parts of the Fermi contour require a different choice of the inner potential in order to bring them into good agreement with the Fermi surface. However, an increase of the inner potential at higher energies, as figure 3(b) suggests to be appropriate, is in contradiction to earlier LEED results and to the general theory of the exchange–correlation potential [23, 32]. An alternative explanation for the need to use different inner potentials for different parts of the Fermi surface is that our model for the potential step at the surface (a step) is inadequate to describe the refraction correctly. This was already found to be a problem when comparing the

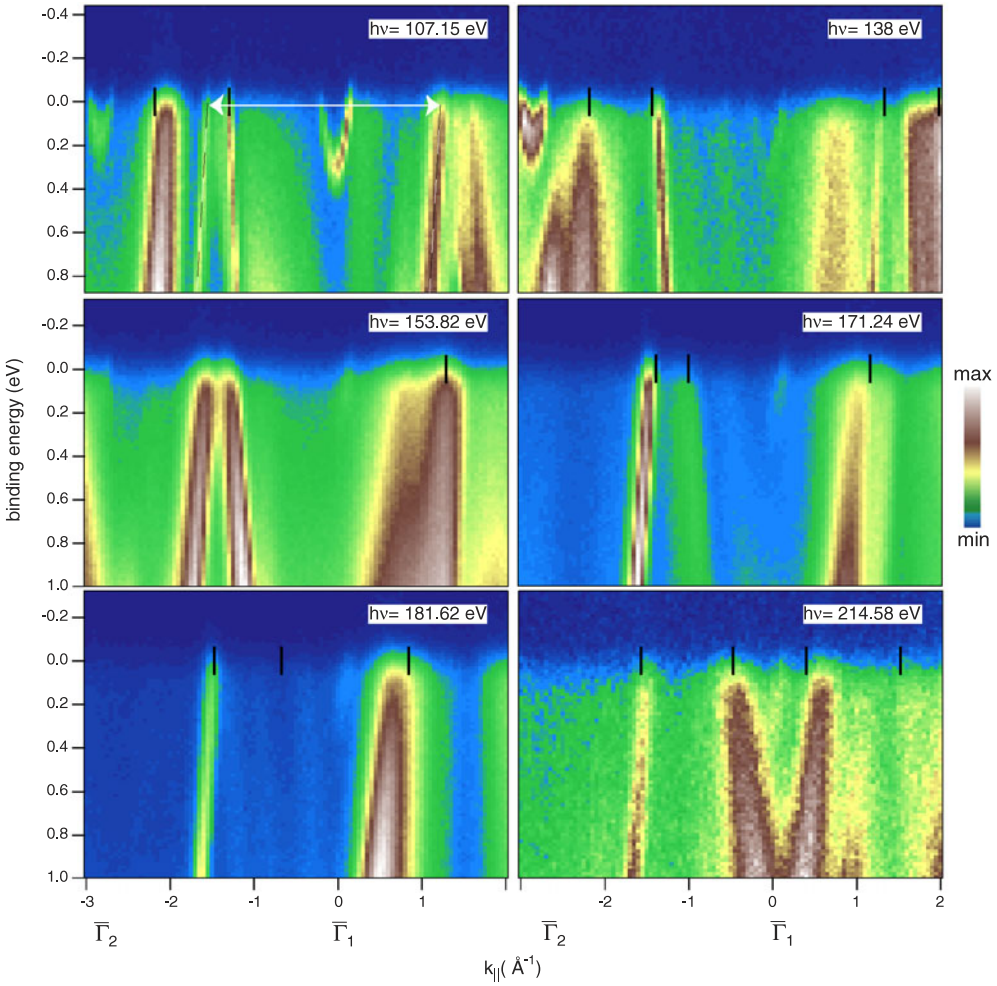

Figure 5. Photoemission intensity as a function of binding energy and $k_{\|}$ for several photon energies. The black markers show the expected Fermi level crossings from the true Fermi surface, using free-electron final states. Equivalent images for the whole data set can be found in the movie which is attached to the online version of this paper at stacks.iop.org/JPhysCM/15/6919/mmedia.

result of a low-energy Fermi surface determination to calculations within the one-step model of photoemission [17].

Motivated by the difficulty of defining a Fermi surface and measuring it in highly correlated narrow-band systems, Straub *et al* [6] have suggested obtaining the Fermi surface from photoemission by taking the maximum of the photoemission intensity gradient $|\nabla_k I(k)|$ instead of the position of the intensity maximum and this method has also been shown to yield improved results for broad-band systems like copper. Figure 4 shows the result of this method, based on the data shown in figure 3(b). This gradient method of determining the Fermi surface produces two Fermi contour lines close to the real Fermi surface; one coincides with the actual Fermi surface, the other is an artefact. Indeed, these double structures can be seen clearly in figure 4, in particular for the surface state Fermi contour near $\bar{\Gamma}_1$. The artefact is known to appear on the occupied side of the Fermi surface which, in our case, is the outside of the

Fermi surface 'butterflies'. This is consistent with most of the observed crossings although the general agreement between the Fermi contour and the true Fermi surface is not good enough to claim a real improvement over the result of figure 3(b). A notable exception is the surface state around $\bar{\Gamma}_1$ where the gradient method considerably improves the Fermi contour position and for which k_F, determined from the interpolated gradient image, is in excellent agreement with the result of high-resolution photoemission at low energies [24]. Obviously, a gradient method is very sensitive to imperfections in the raw data. There are some additional artefacts in figure 4 which are caused by the intensity discontinuities discussed in connection with figure 2. One of these artefacts is marked by a white arrow in figure 4.

Evidently, the bulk-induced photoemission Fermi contour agrees fairly well with the expected Fermi surface. There are, however, several regions where the agreement is less good. In order to understand this better, it is convenient to inspect the individual angular scans and to compare the observed band crossings with the expected positions for the true Fermi surface. For such a comparison we can simply invert the free-electron final state scheme and go from the known k of the bulk Fermi surface to sets of photon energy and $k_\parallel$. This is shown by the black lines in figure 2. Again, we have used an inner potential of 19 eV. From this we can extract the expected Fermi level crossings for every angular scan. Examples at a few photon energies are given in figure 5 and the whole data set is included in the movie attached to the online version of this paper at stacks.iop.org/JPhysCM/15/6919/mmedia.

The measured bulk Fermi surface contours show strong intensity variations, indicating the importance of non-constant matrix elements. For some positions of the bulk Fermi contour we find almost no photoemission intensity in the experiment. The most striking example is the region close to the neck of the Fermi surface at $k_\parallel = 0$ Å^{-1} and $k_\perp \approx 7.5$ Å^{-1}, indicated by a white arrow in figure 3(b). In fact, the band which gives rise to the top left 'butterfly' can be well observed on either side of the region indicated by the arrow but it is completely absent close to the arrow (see figure 5 and movie at stacks.iop.org/JPhysCM/15/6919/mmedia). This strong asymmetry in the intensity is also found in the surface state which is much more intense towards positive $k_\parallel$ values. A similar situation is observed in the upper part of the top right 'butterfly'. One reason why one should not expect a symmetric intensity on both sides of normal emission is the asymmetry in the experimental set-up where the angle between the emission direction and the surface normal is changed but the angle between the polarization vector of the light and the emission direction is constant. This, however, should not lead to such strong effects as we observe close to normal emission. The angular distance between the two surface state Fermi level crossings close to the neck, for instance, is very small.

A more likely explanation is the loss of symmetry which occurs when going away from normal emission. To see this, consider figure 6 which shows a simple free-electron-like band structure with parameters similar to those expected for normal emission from Cu(111), i.e. for the Γ–L direction, in the reduced-zone scheme. The higher bands have been labelled by the reciprocal lattice vector needed to shift them into the first Brillouin zone. In the photoemission event the energy is conserved and the momentum conservation is achieved by adding a reciprocal lattice vector to the initial state momentum. In this way, the direct transitions can be viewed as vertical in the reduced-zone scheme. As an example we have indicated a direct transition at $h\nu = 196$ eV which takes an electron from an initial state close to the L point to a final state in the $\vec{G} = 2\pi/a(2, 2, 2)$ band. We assume that the state with this final state vector propagates in the direction out of the surface normal. When the photon energy is increased, the direct transition will move until it reaches the L point at $h\nu = 208$ eV. For a further increase of the energy the direct transition will move back towards the Γ point, using the $\vec{G} = 2\pi/a(-3, -3, -3)$ band as a final state. This transition cannot be observed since it propagates into the crystal. However, the symmetry between positive and negative

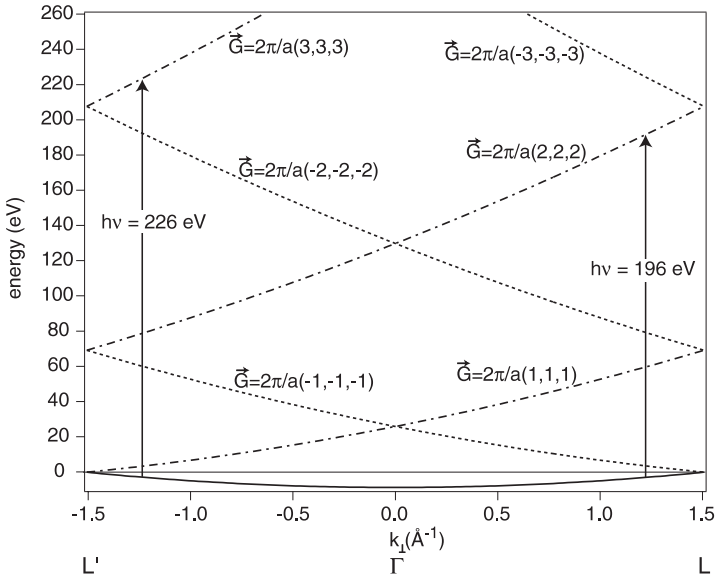

Figure 6. Sketch of a free-electron-type band structure for copper in the reduced-zone scheme. The bands above the Fermi level are labelled according to the reciprocal lattice vector they are shifted by. Two direct transitions are indicated.

$k_\perp$ implies that the equivalent transition from the initial state with negative $k_\perp$, near L′, into the $\vec{G} = 2\pi/a(3, 3, 3)$ final state band can be observed. Such a transition is also shown in the figure at $h\nu = 226$ eV. For off-normal emission, the positive and negative $k_\perp$ directions become non-equivalent and this argument can no longer be applied. Hence one can expect a strong suppression in the intensity of some bands even though direct transitions from them are conserving both momentum and energy. This is what we see in our data. This argument could easily be verified by taking data from surfaces where no such symmetry breaking occurs, for example for the (110) and (100) surfaces.

The asymmetry of the surface state intensity which is most clearly seen in figure 5 and in the movie at stacks.iop.org/JPhysCM/15/6919/mmedia can also be explained in this way and, indeed, confirms the argument given above. For a purely two-dimensional surface, state $k_\perp$ is irrelevant but the Cu(111) Shockley state has some remaining three-dimensional character which leads to a strong energy dependence in its photoemission cross section [26]. The state is derived from the bulk states close to the L point of the Brillouin zone, i.e. the states which form the necks of the Fermi surface. Its intensity asymmetry near the neck is identical to those of these bulk states. The branch with a positive $k_\parallel$ is much more pronounced than the other one.

There is another symmetry argument which is relevant to a situation like ours. We take all the data in a mirror plane of the crystal with the polarization vector also in this mirror plane. In such a case we will be only able to observe photoemission from initial states with even symmetry with respect to a reflection by this mirror plane.

Another discrepancy between the real Fermi surface and our Fermi contour is the presence of strong structures where none should be. This is especially pronounced in the 'neck' connecting the two left 'butterflies'. This neck is not visible but filled with strong bulk photoemission features of apparently distorted Fermi contour segments. A possible explanation is that the Fermi contour is indeed distorted due to the non-free-electron nature of the final

states. Another contribution to this artefact could be the smearing in $k_\perp$. This would be expected to produce such a situation in the vicinity of two almost vertical elements of the Fermi surface. On the other hand, one of the arguments for going to high photon energies was that the $k_\perp$ smearing should be less severe than at low energies. Indeed, if we can estimate the total degree of $k_\perp$ smearing from the full-width half-maximum $\Delta k_\perp$ of the features which have little dispersion in $k_\parallel$. We get $\Delta k_\perp = 0.15$ Å^{-1} as an upper limit for the uncertainty in $k_\perp$ and hence this is not sufficient to explain the disagreement near the left 'neck'.

Another physical mechanism which can produce artefacts in the Fermi contour are (surface) umklapp processes. Examples of these are readily identified in our data set. The most simple case is an umklapp process which involves a surface reciprocal lattice vector along $\bar{\Gamma}$–$\bar{\mathrm{M}}$, i.e. in the direction of our polar scans. Figure 5 shows an example for this in the scan taken at $h\nu = 107.15$ eV. Two dispersing features of exactly the same slope are found which are displaced by a surface reciprocal lattice vector along $\bar{\Gamma}$–$\bar{\mathrm{M}}$. The two dashed black lines which mark the states are parallel and the white arrow represents the length of the surface reciprocal lattice vector. Such umklapp processes are much easier to identify in figure 5 than in the Fermi contour images because one can utilize the dispersion of the states in addition to their position. Another way of viewing the umklapp processes is as additional final state bands in a picture-like figure 6. Indeed, even in the most simple free-electron-like picture there are very many possible final states but most of them are irrelevant because they do not propagate into the emission direction. In normal emission, a restriction to states propagating normal to the surface is justified but in our experiment other final states could be much more appropriate as higher off-normal angles are reached.

The results shown above demonstrate that the approach presented here can be a useful aid for the determination of three-dimensional Fermi surfaces by ARPES. The use of high energies and our strategy of k sampling allows us to map significant fractions of the Fermi surface and to interpolate them in a two-dimensional plane using known final states. As one may expect from the results obtained from low-energy ARPES on copper [30], the use of free-electron final states and the smearing in $k_\perp$ do not lead to severe problems. In fact, using free-electron final states should be more appropriate at these high energies. On the other hand, a careful inspection of figure 3 raises the question of whether the technique is good enough to determine a totally unknown Fermi surface. 'Missing parts' of the Fermi surface as well as spurious features are not unexpected for the reasons explained above. Indeed, they have also been observed in scanned-angle Fermi surface determinations at low energies [3, 6, 13, 14, 16, 17]. However, it would be desirable to understand these remaining discrepancies between our experiment and the well-known bulk Fermi surface in more detail. One way for substantial progress would be to compare our results with calculations performed within the one-step model of photoemission which yield good quantitative agreement with the results from scanned-angle Fermi surface determinations at low energies [17]. As indicated above, it would also be interesting to perform similar measurements on the (100) and (110) surfaces of copper to see if this can reduce the cross section difference for the various segments of the Fermi surface at off-normal emission angles.

Phonon scattering in the final state appears to be fairly insignificant apart from the highest energies where a broadening of the transitions is clearly visible in the Fermi contour maps and in the angular scans. These problems can be overcome by cooling the sample except in cases of very low Debye temperatures. It is curious that the surface state around the $\bar{\Gamma}$ point appears to be observable up to rather high energies, which is most clearly seen in its Fermi contour. This is consistent with recent observations from Al(100) where the surface state could be observed up to energies of several hundred electronvolts [18]. Another interesting point is that we had to increase the inner potential for the free-electron final states from the value usually employed

in ARPES from Cu in order to obtain good agreement with the known Fermi surface. The reason for this is not entirely clear. It could be useful to map the energy and dispersion of the higher unoccupied states in copper by VLEED [11].

4. Conclusions

In conclusion, we have shown that high-energy ARPES can be used to map the Fermi surface of copper. Our results are in reasonable agreement with the well-known bulk Fermi surface but suffer to a small degree from missing Fermi contour features and spurious structures. The origin of these problems and possibly their removal could be understood better by comparing our data to more advanced calculations. Extending ARPES to high energies well beyond the classical VUV regime will clearly add to the tool kit of band structure and Fermi surface determination.

Acknowledgments

This work was supported by the European Community under contract number HPRI-CT-1999-00033 and by the Danish National Research Council. The authors wish to thank V N Strocov for stimulating discussions.

References

[1] Wosnitza J 1996 *Fermi Surfaces of Low-Dimensional Organic Metals and Superconductors* (Berlin: Springer)
[2] Santoni A, Terminello L J, Himpsel F J and Takahashi T 1991 *Appl. Phys.* A **52** 299–301
[3] Aebi P, Osterwalder J, Fasel R, Naumovic D and Schlapbach L 1994 *Surf. Sci.* **307–309** 917–21
[4] Aebi P, Osterwalder J, Schwaller P, Schlapbach L, Shimoda M, Mochiku T and Kadowaki K 1994 *Phys. Rev. Lett.* **72** 2757–60
[5] Avila J, Huttel Y, Mascaraque A, Le Lay G, Michel E G and Asensio M C 1999 *Surf. Sci.* **433–435** 327–31
[6] Straub T, Claessen R, Steiner P, Hüfner S, Eyert V, Friemelt K and Bucher E 1997 *Phys. Rev.* B **55** 13473–8
[7] Kipp L, Roßnagel K, Solterbeck C, Strasser T, Schattke W and Skibowski M 1999 *Phys. Rev. Lett.* **83** 5551–4
[8] Borisenko S V, Kordyuk A A, Legner S, Dürr C, Knupfer M, Golden M S, Fink J, Nenkov K, Eckert D, Yang G, Abell S, Berger H, Forro L, Liang B, Maljuk A, Lin C T and Keimer B 2001 *Phys. Rev.* B **64** 094513
[9] see for example Rotenberg E and Kevan S D 1998 *Phys. Rev. Lett.* **80** 2905
Agergaard S, Søndergaard C, Li H, Nielsen M B, Hoffmann S V, Li Z and Hofmann P 2001 *New J. Phys.* **3** 15.1–15.10
[10] Hüfner S 1996 *Photoelectron Spectroscopy* (Berlin: Springer)
[11] Strokov V N, Claessen R, Nicolay G, Hüfner S, Kimura A, Harasawa A, Shin S, Kakizaki A, Nilsson P O, Starnberg H I and Blaha P 1998 *Phys. Rev. Lett.* **81** 4943
Strokov V N, Claessen R, Nicolay G, Hüfner S, Kimura A, Harasawa A, Shin S, Kakizaki A, Nilsson P O, Starnberg H I and Blaha P 2001 *Phys. Rev.* B **63** 205108
[12] Matzdorf R 1998 *Surf. Sci. Rep.* **30** 153–206
[13] Avila J, Casado C, Asensio M C, Perez J L, Munõz M C and Soria F 1995 *J. Vacuum Sci. Technol.* A **13** 1501–5
[14] Qu Z, Goonewardene A, Subramanian K, Karunamuni M N, Ye J L, Stockbauer R L and Kurtz R 1995 *Surf. Sci.* **524** 133
[15] Rotenberg E, Denlinger J D, Kevan S D, Goodman K W, Tobin J G, Mankey G J and Subramanian K 1996 *Applications of Synchrotron Radiation Techniques to Materials Science III (San Francisco, CA April 1996)* (*Materials Research Society Symp. Proc.* vol 437) ed L J Terminello, S M Mini, H Ade and D L Perry (Pittsburgh, PA: Materials Research Society) pp 47–5
[16] Stampfl A P J, Con Foo J A, Leckey R C G, Riley J D, Denecke R and Ley L 1995 *Surf. Sci.* **331** 1272
[17] Lindroos M, Avila J, Daávila M E, Huttel Y, Asensio M C and Bansil A 2001 *Surf. Sci.* **482–485** 718
[18] Hofmann Ph, Søndergaard Ch, Agergaard S V, Gayone J E, Moreno M S, Zampieri G, Lizzit S and Baraldi A 2002 *Phys. Rev.* B **66** 245422
[19] Søndergaard C, Hofmann Ph, Schultz C, Moreno M S, Gayone J E, Vicente Alvarez M A, Zampieri G, Lizzit S and Baraldi A 2001 *Phys. Rev.* B **63** 233102

[20] Rossnagel K, Kipp L, Skibowski M, Solterbeck C, Strasser T, Schattke W, Voß D, Kruüger P, Mazur A and Pollmann J 2001 *Phys. Rev.* B **63** 125104
[21] Baraldi A, Comelli G, Lizzit S, Kiskinova M and Paolucci G 2003 *Surf. Sci. Rep.* **49** 169
[22] Abrami A, Barnaba M, Battistello L, Bianco A, Brena B, Cautero G, Chen H, Cocco Q D, Comelli G, Contrino S, DeBona F, Di Fonzo S, Fava C, Finetti P, Furlan P, Galimberti A, Gambitta A, Giuressi D, Godnig R, Jark W, Lizzit S, Mazzolini F, Melpignano P, Olivi L, Paolucci G, Pugliese R, Qian S N, Rosei R, Sandrin G, Savoia A, Sergo R, Sostero G, Tommasini R, Tudor M, Vivoda D, Wei F-Q and Zanini F 1995 *Rev. Sci. Instrum.* **66** 1618–20
[23] Lindgren S Å, Waldén L, Rundgren J and Westing P 1984 *Phys. Rev.* B **29** 576
[24] Reinert F, Nicolay G, Schmidt S, Ehm D and Hüfner S 2001 *Phys. Rev.* B **63** 115415
[25] Søndergaard Ch 2001 *PhD Thesis* University of Aarhus
[26] Louie S G, Thiry P, Pinchaux R, Pétroff Y, Chanderis D and Lecante J 1980 *Phys. Rev. Lett.* **44** 549–53
[27] Shevchik N J 1977 *J. Phys. C: Solid State Phys.* **10** L555–7
Shevchik N J 1977 *Phys. Rev.* B **16** 3428–42
Shevchik N J 1979 *Phys. Rev.* B **20** 3020–9
[28] Hellwege K-H and Olsen J L (ed) 1973 *Landoldt–Börnstein New Series* Group III, vol 13 (Berlin: Springer)
[29] Kamm G N 1970 *Phys. Rev.* B **1** 554
[30] Courths R and Hüfner S 1984 *Phys. Rep.* **112** 53
[31] Strocov V N, Claessen R, Aryasetiawan F, Blaha P and Nilsson P O 2002 *Phys. Rev.* B **66** 195104
[32] Rundgren J 1999 *Phys. Rev.* B **59** 5106